

# Reexamination of microscopic optical potentials based on multiple scattering theory

Kosho Minomo,<sup>1,\*</sup> Kouhei Washiyama,<sup>2</sup> and Kazuyuki Ogata<sup>1</sup>

<sup>1</sup>Research Center for Nuclear Physics, Osaka University, Ibaraki 567-0047, Japan

<sup>2</sup>Center for Computational Sciences, University of Tsukuba, Tsukuba 305-8577, Japan

(Dated: January 1, 2018)

**Background:** Microscopic optical potentials have been successful in describing nucleon-nucleus and nucleus-nucleus scattering. Some essential ingredients of the framework, however, have not been examined in detail.

**Purpose:** Applicability of the microscopic folding model is systematically investigated. Effect of an anti-symmetrization factor (ASF) appearing in multiple scattering theory, theoretical uncertainty regarding the local density approximation (LDA), and the validity of a prescription for nonlocality, the Brieva-Rook (BR) localization, of the microscopic potential, are quantitatively estimated for nucleon-nucleus scattering; investigation on the ASF is carried out for also deuteron-nucleus scattering.

**Methods:** A single folding model with the Melbourne  $g$ -matrix interaction and the SLy4 Skyrme-type Hartree-Fock-Bogoliubov (SLy4-HFB) density is employed for evaluating a nucleon-nucleus microscopic optical potential. Deuteron-nucleus scattering is described by the continuum-discretized coupled-channels method incorporating the microscopic proton-nucleus and neutron-nucleus potentials.

**Results:** The ASF is found to affect proton total reaction cross sections  $\sigma_R$  for a  $^{12}\text{C}$  target below 200 MeV by about 10%. Effect of the ASF on  $\sigma_R$  is negligibly small if a target nucleus is heavy or scattering energy is above 200 MeV; elastic cross sections are hardly affected by the ASF for all the reaction systems considered. Below 65 MeV, still the BR localization works quite well. However, at energies below about 50 MeV, the LDA becomes less accurate for evaluating elastic cross sections at backward angles. This is the case also for  $\sigma_R$  of  $p$ - $^{12}\text{C}$  below about 200 MeV.

**Conclusions:** The microscopic model is applicable to nucleon-nucleus scattering above 25 MeV for target nuclei in a wide range of mass numbers. Deviation of calculated results from experimental data is less than about 10%.

PACS numbers: 24.10.Ht, 24.10.Eq, 25.40.Cm, 25.45.De

## I. INTRODUCTION

Construction of optical potentials, which describe a one-body potential between a projectile and a target nucleus for elastic scattering, is one of the most fundamental subjects in nuclear reaction theory. For nucleon-nucleus scattering, some global optical potentials have been constructed phenomenologically by means of the rich data of differential cross sections, total reaction cross sections, and spin observables. Koning and Delaroche proposed a global optical potential for proton and neutron scattering up to 200 MeV in a traditional way, in which the local Woods-Saxon and its derivative forms are assumed [1]. The Dirac phenomenology provides precise optical potentials for proton scattering [2, 3], at higher incident energies in particular. Very recently, nonlocal optical potentials, which well reproduce the measured data even at very low energies, have been constructed with the dispersive optical model [4]. Thus, reliable optical potentials were obtained for proton-nucleus elastic scattering as far as the data are available. Optical potentials are applied to also analysis of other reaction processes, for example, inelastic scattering, breakup, and transfer reactions.

Recently, microscopic approach to optical potentials took large steps. The  $g$ -matrix folding model is one of the most practical methods to construct an optical potential. In the model, the folding potential is obtained by folding a  $g$ -matrix

interaction, which is an effective nucleon-nucleon interaction in nuclear matter, with a target density. Basically,  $g$ -matrix interactions are obtained by solving the Bethe-Bruckner-Goldstone equation. Up to now, many types of  $g$ -matrix interactions have been developed, for example, JLM [5], M3Y and its modified versions (DDM3Y and CDM3Y) [6–8], CEG [9], and Melbourne [10] are often used.

As a noteworthy achievement, the folding calculation with the Melbourne  $g$ -matrix interaction can reproduce the measured cross sections for nucleon-nucleus scattering with no free adjustable parameter [10, 11]. In addition to the conventional nucleon-nucleon interactions, modern interactions including three-body-force (3BF) effects have been developed [12–15]. Those interactions are also used to investigate the 3BF effects for nucleus-nucleus scattering [16, 17] and proton knockout reactions [18]; the 3BF effects are found not to be essential for nucleon-nucleus elastic scattering. Furthermore, great efforts have been done to derive optical potentials by *ab initio* approach, though it is still restricted to reaction systems containing a very limited number of nucleons [19]. Inspired by the pioneering and state-of-the-art microscopic studies by the Melbourne group, several works have been reported for microscopically describing not only nucleon-nucleus scattering but also nucleus-nucleus scattering and other reaction processes. In some cases three-body or four-body reaction models incorporating microscopic distorting potentials are employed [20–23]. In these studies, single- or double-folding model with the Melbourne  $g$ -matrix interaction was adopted, with the local density approximation (LDA) and the localization prescription proposed by Brieva

\*minomo@rcnp.osaka-u.ac.jp

and Rook [24–26], that is, the BR localization. However, applicability of this microscopic framework has not been investigated systematically, at energies below 65 MeV and above 200 MeV in particular. Discussion on the role of an antisymmetrization factor (ASF) (see Sec. II) appearing in multiple scattering theory is also missing. Furthermore, the applicability of the LDA and the BR localization has been examined only in very limited cases. It should be noted that in the original work by the Melbourne group nonlocal terms have explicitly been treated without using the BR localization.

In this study we carry out systematic studies on the applicability of the folding model with the LDA and the BR localization. Properties of its ingredients, that is, the ASF, theoretical uncertainty regarding the LDA, and the validity of the BR localization, are investigated. We mainly focus on proton-nucleus scattering; the role of the ASF is discussed also for deuteron-nucleus scattering by means of the continuum-discretized coupled-channels method (CDCC) [27–29].

The contents of this paper are organized as follows. In Sec. II, we show a theoretical framework and the Schrödinger equation to be solved. The results of nucleon elastic scattering and total reaction cross sections in Secs. III A and III B, respectively. In Sec. III C, we evaluate the theoretical ambiguity of LDA in the  $g$ -matrix folding model, and in Sec. III D, we check the nonlocality of the microscopic optical potential. Application of the microscopic optical potentials for deuteron scattering is shown in Sec. III E. Finally, Sec. IV is devoted to a summary.

## II. THEORETICAL FRAMEWORK

### A. Schrödinger equation with an effective interaction

We consider nucleon (N) scattering from a target nucleus (T) with mass number  $A_T$ . A theoretical foundation of the  $g$ -matrix folding model is given by multiple scattering theory [30]. We start with the following Schrödinger equation described by a bare nucleon-nucleon interaction between N and a  $j$ -th nucleon in T,  $v_j$ ,

$$\left[ K + h_T + \sum_{j \in T} v_j - E \right] \Psi = 0. \quad (1)$$

Here,  $E$  is the total energy,  $K$  is the kinetic energy operator between N and T,  $h_T$  is the internal Hamiltonian of T.  $\Psi$  is the total wave function. Multiple scattering theory allows one to solve the following equation with an effective interaction  $\tau_j$ ,

$$\left[ K + h_T + \frac{A_T - 1}{A_T} \sum_{j \in T} \tau_j - E \right] \hat{\Psi} = 0, \quad (2)$$

instead of solving Eq. (1). The transition matrix  $T$  for elastic scattering is given by

$$T = \frac{A_T}{A_T - 1} T', \quad (3)$$

where  $T'$  is the transition matrix obtained by solving Eq. (2).  $(A_T - 1)/A_T$  in Eq. (2) and  $A_T/(A_T - 1)$  in Eq. (3) appear as a result of antisymmetrization in multiple scattering theory; below we call each of them an antisymmetrization factor (ASF).

With the nuclear matter approximation for implementing the medium effects in  $\tau_j$ , it is replaced with a  $g$ -matrix interaction. Multiplying Eq. (2) by a target ground-state wave function from the left, a one-body Schrödinger equation for the relative motion between N and T for elastic scattering is derived:

$$\left[ K_{\mathbf{R}} + \frac{A_T - 1}{A_T} U(\mathbf{R}) + U_{\text{Coul}}(\mathbf{R}) - E_{\text{c.m.}} \right] \chi(\mathbf{R}) = 0. \quad (4)$$

Here,  $U(\mathbf{R})$  is a localized folding potential between N and T, which consists of the central and spin-orbit parts; the explicit form is given in Ref. [31].  $U_{\text{Coul}}$  is the Coulomb potential and  $E_{\text{c.m.}}$  is the incident energy in the center-of-mass frame.

The total reaction cross section  $\sigma_R$  is given by

$$\sigma_R = \frac{\pi}{k^2} \sum_{L,J} (2J+1)(1 - |S_{LJ}|^2), \quad (5)$$

where

$$S_{LJ} = -\frac{1}{A_T - 1} + \frac{A_T}{A_T - 1} S'_{LJ}. \quad (6)$$

Here,  $S'_{LJ}$  is the scattering matrix obtained by solving Eq. (4), and  $k$  is the relative wave number between N and T.  $L$  ( $J$ ) is the orbital (total) angular momentum appeared in the partial-wave decomposition of  $\chi$ .

The ASFs have been ignored in most cases. However, these may play an important role when lighter targets are involved. It should be noted that no ASF appears when a phenomenological optical potential is considered.

### B. Three-body model

In Refs. [22, 23] multiple scattering theory was applied to deuteron scattering. The weakly bound property of deuteron allows one to adopt a three-body reaction model and the Schrödinger equation is given by

$$\left[ K + h_d + \frac{A-1}{A} (U_{pT} + U_{nT}) - E_{\text{c.m.}} \right] \chi = 0. \quad (7)$$

Here,  $h_d$  is the internal Hamiltonian of deuteron and  $U_{pT}$  ( $U_{nT}$ ) is a distorting potential between proton (neutron) and the target obtained microscopically.  $A$  is the product of the mass numbers of deuteron and target nucleus, that is,  $A = 2A_T$ . In the previous studies [22, 23] the ASF  $(A-1)/A$  was disregarded, validity of which is examined in Sec. III E. The three-body equation (7) is solved by using the continuum-discretized coupled-channels method (CDCC) [27–29].

### C. Skyrme Hartree-Fock-Bogoliubov density

The one-body densities used in our microscopic optical potential are calculated within the Hartree-Fock-Bogoliubov (HFB) model with SLy4 Skyrme energy density functionals [32]. In the pairing channel, we use mixed-type pairing functionals with a quasiparticle cutoff of 60 MeV. The pairing strength is determined so as to reproduce the neutron pairing gap of 1.25 MeV in  $^{120}\text{Sn}$ . We use the computer code LENTEUR [33], where one-body HFB equations are solved in spherical symmetry and time-reversal symmetry. Odd and odd-odd nuclei are calculated by constraining average particle numbers to its odd numbers without breaking time-reversal symmetry.

### III. RESULTS AND DISCUSSION

In this paper, we calculate proton scattering on  $^{12}\text{C}$ ,  $^{40}\text{Ca}$ , and  $^{208}\text{Pb}$  from 25 to 800 MeV. For comparison, we adopt two types of target densities. One is SLy4-HFB density as explained in Sec. III C, and the other is the phenomenological one deduced from the analysis of electron scattering [34]. For the latter, the proton density is obtained by unfolding the charge distribution with the finite-size effect of proton charge [35], and the neutron densities for  $^{12}\text{C}$  and  $^{40}\text{Ca}$  are approximated to be the same as those of proton; for  $^{208}\text{Pb}$ , we adopt the neutron density distribution deduced from the analysis of proton elastic scattering [36]. We refer the phenomenological density as the Sum-of-Gaussian (SOG) density below.

We use the Melbourne  $g$ -matrix interaction [10]. At energies higher than 300 MeV, we adopt the  $g$ -matrices with the optical model prescription (OMP) [37] that modify the bare interaction to implement the meson production effects. The relativistic correction for the kinematics is considered in solving Eq. (4), that is, the wave number is estimated according to the relativistic kinematics and we take the reduced energy instead of the reduced mass.

#### A. Nucleon elastic scattering

Figure 1 shows the differential cross sections for  $p$ - $^{12}\text{C}$  elastic scattering from 26 to 200 MeV. The solid (dashed) lines correspond to the results using the microscopic density with (without) the ASF. The dotted lines represent the result with the SOG density and the ASF. It is found that the ASF shifts the diffraction pattern to backward angles very slightly. This effect becomes smaller as the incident energy increases since  $(A_T - 1)/A_T$  in Eq. (2) and  $A_T/(A_T - 1)$  in Eq. (3) are almost canceled. This indicates multistep processes in terms of  $U$  become less important at higher energies, as expected in Ref. [30].

Comparing the results with the two types of densities, the difference is negligibly small at low energies, whereas it appears at large angles at higher energies. Agreement between the theoretical results and the experimental data are satisfactorily well at 26, 35, and 50 MeV, except around the dips. At

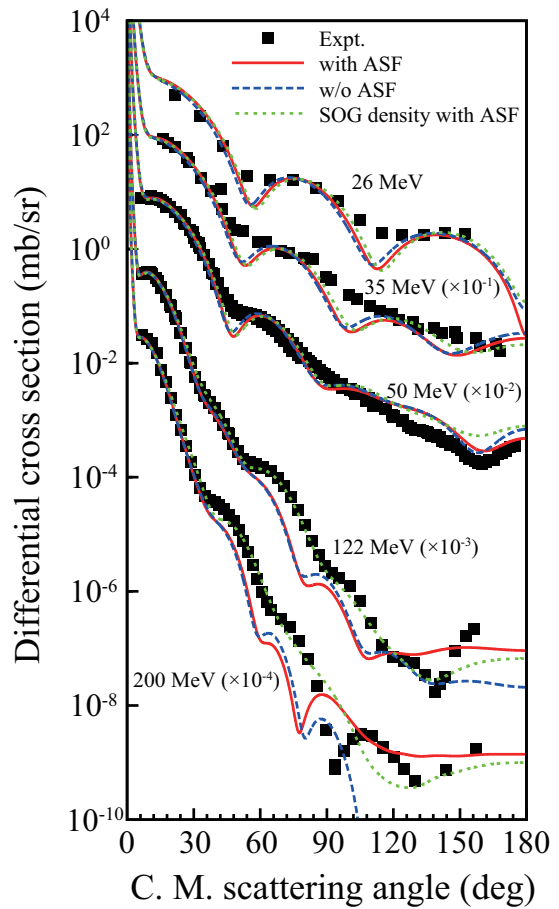


FIG. 1: (Color online) Differential cross sections for  $p$ - $^{12}\text{C}$  elastic scattering as a function of the scattering angle in the center-of-mass frame. The solid and dashed lines show the results obtained with the microscopic density with and without the ASFs, respectively, whereas the dotted lines correspond to the result with the SOG density and the ASF. The incident energies are 26, 35, 50, 122, and 200 MeV from the top to the bottom, and the results are scaled for visibility by the factors in parentheses near the curves. The experimental data are taken from Refs. [38–45].

higher energies, the dotted lines retain this feature, whereas the other two show some deviation at backward angles. This indicates that  $^{12}\text{C}$  is too light for the SLy4-HFB calculation to describe its density distribution, in the nuclear interior region in particular. It will be worth pointing out that even in this situation the cross sections calculated with the SLy4-HFB density agree well with the data at forward angles, in which the cross sections are dominantly large.

Features of the results for  $^{40}\text{Ca}$  and  $^{208}\text{Pb}$  targets, shown in Figs. 2 and 3 respectively, are quite similar to those in Fig. 1 except that i) the ASF little affect the results and ii) the two densities give almost the same cross sections even at high energies. Consequently, the results with the SLy4-HFB density reproduce the experimental data very well; at larger angles for scattering on  $^{208}\text{Pb}$  still the results with the SOG density gives a slightly better agreement. The overshooting at backward an-

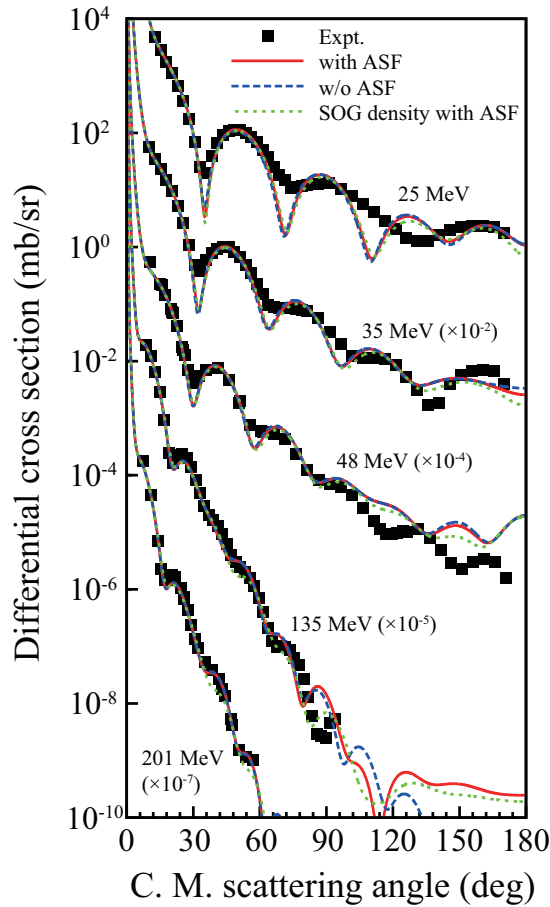


FIG. 2: (Color online) Differential cross sections for  $p$ - $^{40}\text{Ca}$  elastic scattering. The meaning of the lines is same as that in Fig. 1. The experimental data are taken from Refs. [46–48].

gles at low energies in Fig. 3 may be due to the Coulomb excitation that is not taken into account in the present calculation.

Figure 4 shows the differential cross sections for proton elastic scattering from  $^{12}\text{C}$ ,  $^{40}\text{Ca}$ , and  $^{208}\text{Pb}$  at 500 and 800 MeV. Results with the SLy4-HFB density neglecting the ASF are found to completely agree with those with the ASF and thus not plotted. Although the agreement between the theoretical and experimental results is not bad at very forward angles, the diffraction pattern of the theoretical calculations shifts to forward angles compared with that of the data. The SOG density gives slightly better agreement with the experimental data but still it somewhat deviates from the data. This may suggest a limitation of the nonrelativistic approach to high energy scattering.

### B. Total reaction cross sections for nucleon scattering

Figure 5 shows the total reaction cross sections  $\sigma_R$  for  $p$ - $^{12}\text{C}$  scattering, as a function of the incident energy. The closed

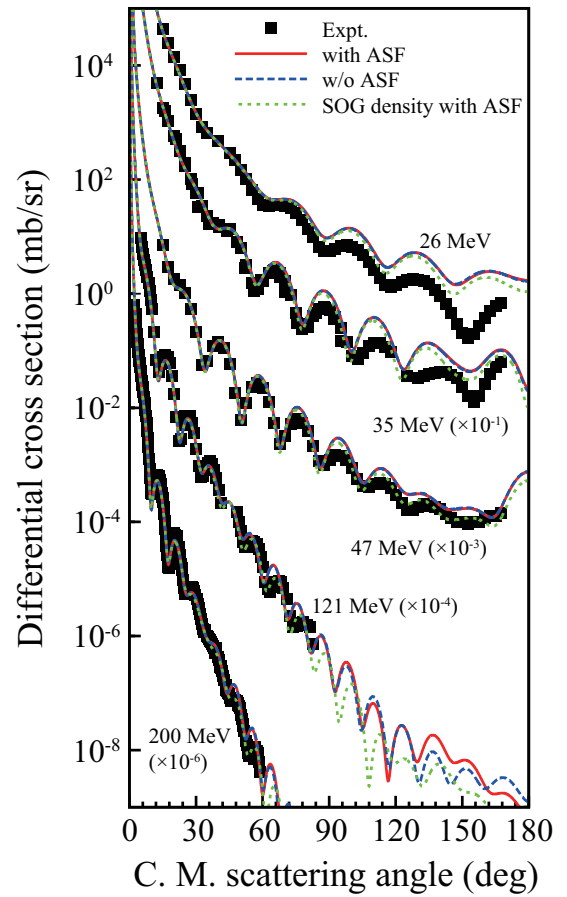


FIG. 3: (Color online) Differential cross sections for  $p$ - $^{208}\text{Pb}$  elastic scattering. The meaning of the lines is same as that in Fig. 1. The experimental data are taken from Refs. [47, 49–51].

(open) circles correspond to the results with (without) the ASF and the triangles to the results with the SOG density including the ASF. The lines are guides for eyes. The experimental data are taken from Refs. [59–64].

At low energies, there is a 10% difference between the results with and without the ASF, and the former shows a better agreement with the experimental data. This difference disappears at energies higher than 200 MeV. It is found that  $\sigma_R$  calculated with the SOG density is smaller than that with the SLy4-HFB density by several percent. This difference reflects the larger matter RMS radius of the Sly4-HFB density than that of the SOG density.

Figures 6 and 7 show  $\sigma_R$  for  $p$ - $^{40}\text{Ca}$  and  $p$ - $^{208}\text{Pb}$  scattering, respectively. For the former, the effect of the ASF is significantly smaller than in Fig. 5, whereas for the latter the effect is totally negligible. In both cases, the two densities give almost the same results.  $\sigma_R$  for  $p$ - $^{40}\text{Ca}$  slightly overshoots the experimental data. For  $p$ - $^{208}\text{Pb}$  the agreement with the data is quite satisfactory except the undershooting below about 50 MeV.

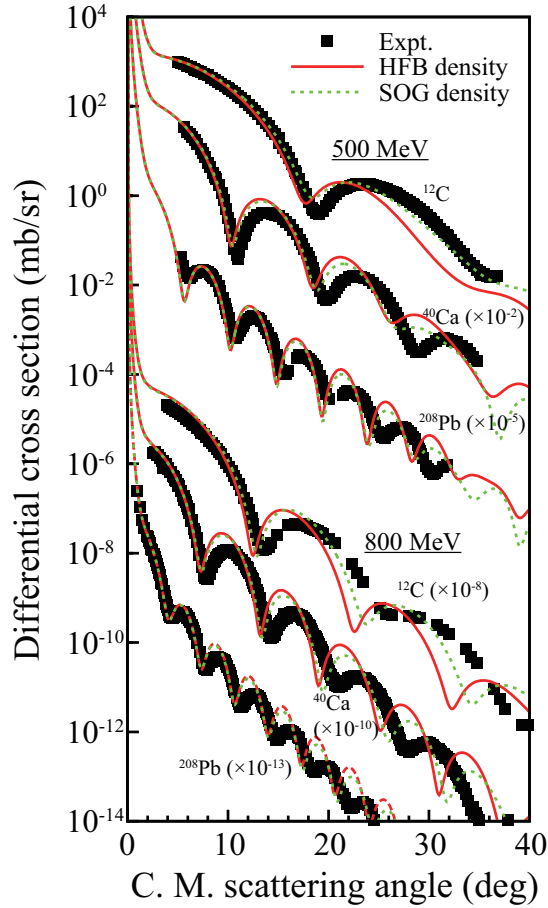


FIG. 4: (Color online) Differential cross sections for proton elastic scattering from  $^{12}\text{C}$ ,  $^{40}\text{Ca}$ , and  $^{208}\text{Pb}$  at high energies. The incident energies of the three results from the top correspond to around 500 MeV, and the lower three to 800 MeV. The solid (dotted) line shows the result with the SLy4-HFB (SOG) density including the ASF. The experimental data are taken from Refs. [52–58].

### C. Theoretical ambiguity coming from the local density approximation

The  $g$ -matrix interaction is applied to finite nuclei with the local density approximation (LDA), that is, we choose the density at a certain point,  $r_g$ , as the density-dependence of the  $g$ -matrix interaction in the folding procedure. We have three choices for  $r_g$ : i) the mid point of the interacting two nucleons ( $r_m$ ), ii) the coordinate of the internal nucleon ( $r$ ), and iii) that of the incoming nucleon ( $R$ ). If the LDA is completely valid, the calculated results are independent of the choice of  $r_g$ . By comparing the results with ii) and iii), which correspond to the two extreme cases, we can estimate how large the theoretical ambiguity of the LDA is at most. In this paper we consider the scattering below 65 MeV; for energies above 65 MeV, see Ref. [69].

Figure 8 shows the differential cross sections for  $p$ - $^{12}\text{C}$  and  $p$ - $^{208}\text{Pb}$  scattering calculated with the different choices of  $r_g$ .

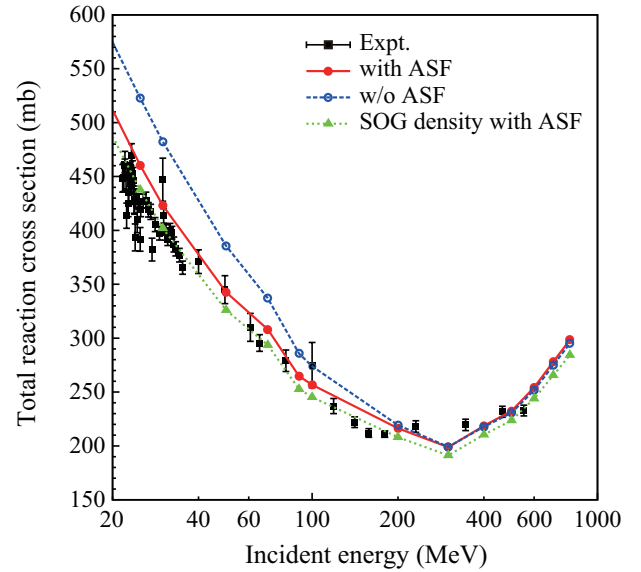


FIG. 5: (Color online) Energy dependence of the total reaction cross sections for  $p$ - $^{12}\text{C}$  scattering. The closed (open) circles correspond to the result with (without) the ASF and the triangles to the results with the SOG density including the ASF. The lines are guides for eyes. The experimental data are taken from Refs. [59–64].

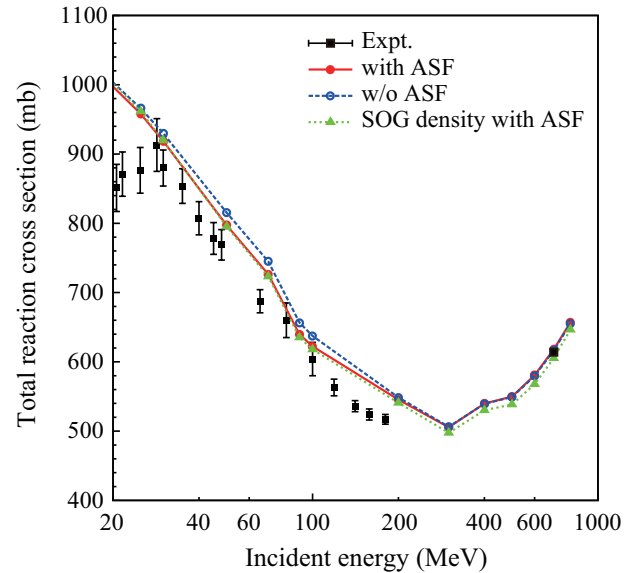


FIG. 6: (Color online) Same as Fig. 5 but for  $p$ - $^{40}\text{Ca}$ . The experimental data are taken from Refs. [61, 62, 65–68].

The solid, dashed, and dotted lines correspond to i)  $r_g = r_m$ , ii)  $r_g = r$ , and iii)  $r_g = R$ , respectively. The experimental data are taken from Refs. [42, 49, 70–73]. below 50 MeV, the diffraction pattern varies by changing  $r_g$ . Features of the results seem not to depend on the target nuclei. At 65 MeV, the density-dependence of the  $g$ -matrix itself becomes relatively weak so that the three lines agree quite well each other; this is

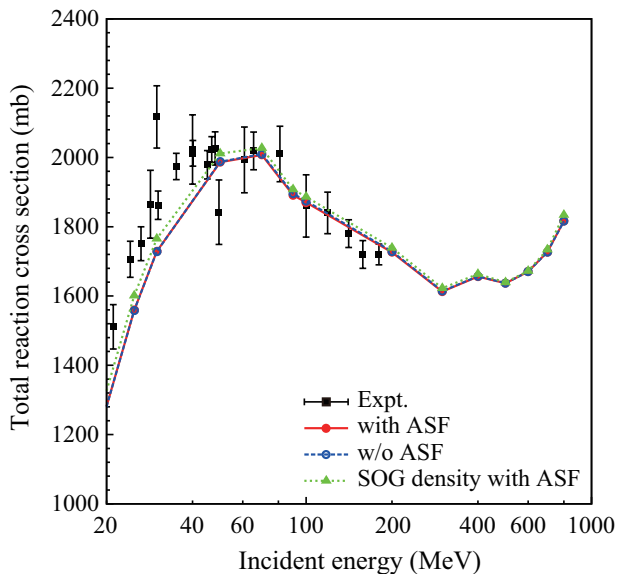


FIG. 7: (Color online) Same as Fig. 5 but for  $p$ - $^{208}\text{Pb}$ . The experimental data are taken from Refs. [60–62, 66, 67].

consistent with the finding in Ref. [69] above 65 MeV.

A similar investigation on  $\sigma_R$  for  $p$ - $^{12}\text{C}$  and  $p$ - $^{208}\text{Pb}$  is shown in Fig. 9. The open circles, the closed circles, and the triangles represent the results corresponding to choices i), ii), and iii), respectively. For each system, the three results are different from each other by several percent below 200 MeV. The small but finite difference will indicate the theoretical uncertainty from the use of the LDA, even though the uncertainty may be overestimated in the present analysis.

#### D. Treatment of nonlocality

In general, microscopic optical potentials are nonlocal due to the antisymmetrization between the incoming and internal nucleons. It was shown in Ref. [69] the nonlocal effects can be well treated by a localization prescription proposed in Refs. [24–26], that is, the Brieva-Rook (BR) localization, for proton elastic scattering on a  $^{90}\text{Zr}$  target. In this study we examine the validity of the BR localization for the calculation of the elastic cross sections for  $p$ - $^{12}\text{C}$  and  $p$ - $^{208}\text{Pb}$  at 30 MeV (Fig. 10),  $\sigma_R$  for these at 30, 65, and 100 MeV (Table I), and the scattering wave functions (Fig. 11). In the calculation, only the central part of the potential is included and we take  $r_g = r$  as the density-dependence of the  $g$ -matrix interaction. We use the target ground-state wave function obtained by the spherical Hartree-Fock calculation with the Gogny D1S interaction.

In Figure 10, we show the cross sections for  $p$ - $^{12}\text{C}$  and  $p$ - $^{208}\text{Pb}$  at 30 MeV. The solid (dashed) line represents the result with the nonlocal (localized) potential. The BR localization is found to work rather well even at low energy. Comparison on  $\sigma_R$  is shown in Table I, which justifies the BR localization for

also  $\sigma_R$  with error about a few percent.

TABLE I: Proton total reaction cross sections  $\sigma_R$  calculated with nonlocal and localized potentials.

	$\sigma_R$ (mb)	
	nonlocal	local
$p$ - $^{12}\text{C}$ @30MeV	441.0	452.2
$p$ - $^{12}\text{C}$ @65MeV	313.5	318.6
$p$ - $^{12}\text{C}$ @100MeV	241.9	244.6
$p$ - $^{208}\text{Pb}$ @30MeV	1697.9	1758.2
$p$ - $^{208}\text{Pb}$ @65MeV	1925.3	1945.2
$p$ - $^{208}\text{Pb}$ @100MeV	1758.2	1766.7

It is known that because of the nonlocality of the distorting potential the amplitude of the scattering wave  $\chi^{(\text{nonlocal})}$  obtained with a nonlocal potential is smaller than that of  $\chi^{(\text{local})}$ , a solution with a localized one in the nuclear interior region. This is called the Perey effect and phenomenologically taken into account by multiplying  $\chi^{(\text{local})}$  by the so-called Perey factor. In this study we take the ratio of  $\chi_L^{(\text{nonlocal})}$  to  $\chi_L^{(\text{local})}$ , and see the radial dependence of the Perey effect in a more direct manner;  $\chi_L^{(\text{nonlocal})}(\chi_L^{(\text{local})})$  is a partial wave of  $\chi^{(\text{nonlocal})}(\chi^{(\text{local})})$  with the angular momentum  $L$  between proton and the target nucleus. To smear the  $L$  dependence, we define an averaged Perey factor by

$$F(R) = \frac{1}{L_{\text{max}} + 1} \sum_{L=0}^{L_{\text{max}}} \frac{\chi_L^{(\text{nonlocal})}(R)}{\chi_L^{(\text{local})}(R)}, \quad (8)$$

where  $L_{\text{max}}$  is the number for the partial waves.

Figure 11 shows the real part of  $F(R)$  for  $p$ - $^{12}\text{C}$  and  $p$ - $^{208}\text{Pb}$  elastic scattering; the imaginary part is almost zero since  $\chi_L^{(\text{nonlocal})}(R)$  and  $\chi_L^{(\text{local})}(R)$  are close to each other for all  $L$ . One sees that  $F(0)$ , which can be regarded as a measure of the nonlocality, does not depend strongly on the target nuclei. On the other hand,  $F(0)$  shows clear dependence on the incident energy. This can be understood by the fact that the exchange term of the interaction, the source of nonlocality in the folding model calculation, has less contribution at higher energies. The range of  $F(R)$  depends on the target, reflecting the range of the exchange term. The Perey effect shown in Fig. 11 must be included in reaction calculations in which a scattering wave calculated with a localized potential is involved, for example, transfer and knockout reactions. It should be noted that  $F(R)$  turns out to depend on NN effective interactions. More detailed studies on  $F(R)$  will be necessary. Investigation on the nonlocality of the spin-orbit term will also be important [74].

#### E. Deuteron scattering

We here investigate the effect of the ASF on deuteron scattering. The model space of CDCC adopted in solving Eq. (7)

is the same as in Ref. [23]. The effect on the deuteron elastic cross section is found to be very similar to that on nucleon scattering discussed in Sec. III A. Figure 12 shows the effect of the ASF on  $\sigma_R$  for  $d$ - $^{12}\text{C}$  scattering. The meaning of the symbols is the same as in Fig. 5. The experimental data are taken from Refs. [75–77]. The results with the global optical potential for deuteron elastic scattering [78], which is applicable up to 91 MeV/nucleon, are shown by the open squares. The effects of the ASF is rather small, because the factor is more close to unity than that for  $p$ - $^{12}\text{C}$ . There is a few percent difference between the SLy4-HFB and SOG densities. However, both results are almost consistent with the measured data and the results with the global optical potential.

#### IV. SUMMARY

We have systematically examined the applicability of the microscopic folding model based on the Melbourne  $g$ -matrix interaction and the SLy4-HFB nuclear density. Effect of the ASF appearing in multiple scattering theory, theoretical uncertainty coming from the LDA, and the validity of the BR localization are investigated in particular. Deuteron-nucleus scattering is also considered to evaluate the effect of the ASF on it; CDCC with nucleon-nucleus microscopic potentials obtained by the folding model is adopted.

We found that the effect of the ASF is about 10% on  $\sigma_R$  for  $p$ - $^{12}\text{C}$  below 200 MeV resulting in better agreement with experimental data, whereas it is negligibly small on  $\sigma_R$  in other cases and on the elastic cross sections in all the cases considered. The ASF should therefore be included in evaluating the microscopic potential as well as the transition amplitude, if the mass number of the target nucleus is small and the scattering energy is low. At low energies, the LDA becomes less reliable and may cast doubt on a  $g$ -matrix folding model and resulting observables. The theoretical uncertainty regarding the LDA

was found to be about 10% at most. One should keep this possible uncertainty in mind when a  $g$ -matrix folding model is applied to scattering at low energies. The BR localization turned out to work quite well even below 65 MeV. The Perey effect on the scattering wave was shown by directly comparing the scattering waves obtained with nonlocal and localized microscopic potentials. Further investigation on the Perey effect, its dependence on the effective NN interactions in particular, will be necessary. Another important finding is that the SLy4-HFB density can be an alternative to a phenomenological density except for light nuclei, for example,  $^{12}\text{C}$ . This will allow one to apply the framework to scattering of unstable nuclei for which a phenomenological density is not available.

Thus, the microscopic folding model employing the Melbourne  $g$ -matrix interaction and the SLy4-HFB density, with the LDA and the BR localization implemented, was found to work satisfactorily well for describing nucleon-nucleus scattering at energies higher than about 25 MeV. Possible deviation from experimental data will roughly be 10%, depending on the reaction systems and observables. A description of scattering at even lower energy will require a new approach, having a wider model space and contains less approximations, beyond the  $g$ -matrix folding model.

#### Acknowledgements

The authors thank S. Karataglidis and K. Amos for valuable discussion. The authors thank Y. S. Neoh for checking the numerical results partly. This work is supported in part by Grant-in-Aid for Scientific Research (Nos. 16K05352 and 16K17698) from Japan Society for the Promotion of Science (JSPS) and by ImpACT Program of Council for Science, Technology and Innovation (Cabinet Office, Government of Japan). The numerical calculations in this work were performed at RCNP.

- 
- [1] A. J. Koning and J. P. Delaroche, Nucl. Phys. A **713**, 231 (2003).
- [2] S. Hama, B. C. Clark, E. D. Cooper, H. S. Sherif, and R. L. Mercer, Phys. Rev. C **41**, 2737 (1990).
- [3] E. D. Cooper, S. Hama, B. C. Clark, and R. L. Mercer, Phys. Rev. C **47**, 297 (1993).
- [4] W. H. Dickhoff, R. J. Charity, and M. H. Mahzoon, arXiv: 1606.08822 (2016).
- [5] J. P. Jeukenne, A. Lejeune, and C. Mahaux, Phys. Rev. C **16**, 80 (1977).
- [6] G. Bertsch, J. Borysowicz, H. McManus, and W. G. Love, Nucl. Phys. A **284**, 399 (1977).
- [7] M. E.-A. Farid and G. R. Satchler, Nucl. Phys. A **438**, 525 (1985).
- [8] D. T. Khoa, G. R. Satchler, and W. von Oertzen, Phys. Rev. C **56**, 954 (1997).
- [9] N. Yamaguchi, S. Nagata, and T. Matsuda, Prog. Theor. Phys. **70**, 459 (1983); N. Yamaguchi, S. Nagata, and J. Michiyama, Prog. Theor. Phys. **76**, 1289 (1986).
- [10] K. Amos, P. J. Dortmans, H. V. Von Geramb, S. Karataglidis, and J. Raynal, in *Advances in Nuclear Physics*, edited by J. W. Negele and E. Vogt (Plenum, New York, 2000) Vol. 25, p. 275.
- [11] P. K. Deb, B. C. Clark, S. Hama, K. Amos, S. Karataglidis and E. D. Cooper, Phys. Rev. C **72**, 014608 (2005).
- [12] T. Furumoto, Y. Sakuragi, and Y. Yamamoto, Phys. Rev. C **78**, 044610 (2008).
- [13] Y. Yamamoto, T. Furumoto, N. Yasutake, and Th. A. Rijken, Phys. Rev. C **88**, 022801 (2013).
- [14] S. Rafi, M. Sharma, D. Pachouri, W. Haider, and Y. K. Gambhir, Phys. Rev. C **87**, 014003 (2013).
- [15] M. Toyokawa, M. Yahiro, T. Matsumoto, K. Minomo, K. Ogata, and M. Kohno, Phys. Rev. C **92**, 024618 (2015); Phys. Rev. C **96**, 059905(E) (2017).
- [16] K. Minomo, M. Kohno, and K. Ogata, Phys. Rev. C **93**, 014607 (2016).
- [17] T. Furumoto, Y. Sakuragi, and Y. Yamamoto, Phys. Rev. C **94**, 044620 (2016).
- [18] K. Minomo, M. Kohno, K. Yoshida, and K. Ogata, Phys. Rev. C **96**, 024609 (2017).
- [19] J. Rotureau, P. Danielewicz, G. Hagen, F. M. Nunes, and T.

- Papenbrock, Phys. Rev. C **95**, 024315 (2017).
- [20] Y. Kikuchi, T. Matsumoto, K. Minomo, and K. Ogata, Phys. Rev. C **88**, 021602 (2013).
- [21] K. Minomo, T. Matsumoto, K. Egashira, K. Ogata, and M. Yahiro, Phys. Rev. C **90**, 027601 (2014).
- [22] Y. S. Neoh, K. Yoshida, K. Minomo, and K. Ogata, Phys. Rev. C **94**, 044619 (2016).
- [23] K. Minomo, K. Washiyama, and K. Ogata, Jour. Nucl. Sci. Technol. **54**, 127 (2017).
- [24] F. A. Brieva and J. R. Rook, Nucl. phys. A **291**, 299 (1977).
- [25] F. A. Brieva and J. R. Rook, Nucl. phys. A **291**, 317 (1977).
- [26] F. A. Brieva and J. R. Rook, Nucl. phys. A **297**, 206 (1978).
- [27] M. Kamimura, M. Yahiro, Y. Iseri, Y. Sakuragi, H. Kameyama, and M. Kawai, Prog. Theor. Phys. Suppl. **89**, 1 (1986).
- [28] N. Austern, Y. Iseri, M. Kamimura, M. Kawai, G. Rawitcher, and M. Yahiro, Phys. Rep. 1987 Oct; 154: 125-204.
- [29] M. Yahiro, K. Ogata, T. Matsumoto, and K. Minomo, Prog. Theor. Exp. Phys. **2012**, 01A206 (2012).
- [30] A. K. Kerman, H. McManus, and R. M. Thaler, Ann. Phys. **8**, 551 (1959).
- [31] M. Toyokawa, K. Minomo, and M. Yahiro, Phys. Rev. C **88**, 054602 (2013).
- [32] E. Chabanat, P. Bonche, P. Haensel, J. Meyer, and R. Schaeffer, Nucl. Phys. A **635**, 231 (1998).
- [33] K. Bennaceur (unpublished).
- [34] H. de Vries, C. W. de Jager, and C. de Vries, At. Data Nucl. Data Tables **36**, 495 (1987).
- [35] R. P. Singhal, M. W. S. Macauley, and P. K. A. De Witt Huberts, Nucl. Instrum. and Method **148**, 113 (1978).
- [36] J. Zenihiro, H. Sakaguchi, T. Murakami, M. Yosoi, Y. Yasuda, S. Terashima, Y. Iwao, H. Takeda, M. Itoh, H. P. Yoshida, and M. Uchida, Phys. Rev. C **82**, 044611 (2010).
- [37] H. V. von Geramb, K. A. Amos, H. Labes, and M. Sander, Phys. Rev. C **58**, 1948 (1998).
- [38] M. Harada, Y. Watanabe, A. Yamamoto, S. Yoshioka, K. Sato, T. Nakashima, H. Ijiri, H. Yoshida, Y. Uozumi, N. Koori, S. Meigo, O. Iwamoto, T. Fukahori, and S. Chiba, Jour. Nucl. Sci. Technol. **36**, 313 (1999).
- [39] E. Fabrici, S. Micheletti, M. Pignatelli, F. G. Resmini, R. De Leo, G. D'Erasmus, and A. Pantaleo, Phys. Rev. C **21**, 844 (1980).
- [40] J. A. Fannon, E. J. Burge, D. A. Smith, and N. K. Ganguly, Nucl. Phys. A **97**, 263 (1967).
- [41] N. M. Clarke, E. J. Burge, and D. A. Smith, Nucl. Phys. A **157**, 145 (1971).
- [42] A. A. Rush, E. J. Burge, and D. A. Smith, Nucl. Phys. A **166**, 378 (1971).
- [43] J. R. Comfort, S. M. Austin, P. T. Debevec, G. L. Moake, R. W. Finlay, and W. G. Love, Phys. Rev. C **21**, 2147 (1980).
- [44] H. O. Meyer, P. Schwandt, W. W. Jacobs, and J. R. Hall, Phys. Rev. C **27**, 459 (1983).
- [45] H. O. Meyer, P. Schwandt, G. L. Moake, and P. P. Singh, Phys. Rev. C **23**, 616 (1981).
- [46] R. H. McCamis, T. N. Nasr, J. Birchall, N. E. Davison, W. T. H. van Oers, P. J. T. Verheijen, R. F. Carlson, A. J. Cox, B. C. Clark, E. D. Cooper, S. Hama, and R. L. Mercer, Phys. Rev. C **33**, 1624 (1986).
- [47] A. Nadasen, P. Schwandt, P. P. Singh, W. W. Jacobs, A. D. Bacher, P. T. Debevec, M. D. Kaitchuck, and J. T. Meek, Phys. Rev. C **23**, 1023 (1981).
- [48] H. Seifert, J. J. Kelly, A. E. Feldman, B. S. Flanders, M. A. Khandaker, Q. Chen, A. D. Bacher, G. P. A. Berg, E. J. Stephenson, P. Karen, B. E. Norum, P. Welch, and A. Scott, Phys. Rev. C **47**, 1615 (1993).
- [49] W. T. H. Van Oers, H. Haw, N. E. Davison, A. Ingemarsson, B. Fagerstroem, and G. Tibell, Phys. Rev. C **10**, 307 (1974).
- [50] W. T. Wagner, G. M. Crawley, G. R. Hammerstein, and H. McManuc, Phys. Rev. C **12**, 757 (1975).
- [51] D. A. Hutcheon, W. C. Olsen, H. S. Sherif, Y. Dymarz, J. M. Cameron, J. Johansson, P. Kitching, P. R. Liljestrang, W. J. McDonald, C. A. Miller, G. C. Neilson, D. M. Sheppard, D. K. McDaniels, J. R. Tinsley, P. Schwandt, L. W. Swensen, and C. E. Stronach, Nucl. Phys. A **483**, 429 (1988).
- [52] G. W. Hoffmann, M. L. Barlett, D. Ciskowski, G. Pauletta, M. Purcell, L. Ray, J. F. Amann, J. J. Jarmer, K. W. Jones, S. Penttila, N. Tanaka, M. M. Gazzaly, J. R. Comfort, B. C. Clark, and S. Hama, Phys. Rev. C **41**, 1651 (1990).
- [53] G. W. Hoffmann, M. L. Barlett, G. Pauletta, L. Ray, J. F. Amann, K. Jones, J. B. McClelland, R. W. Ferguson, M. M. Gazzaly, B. C. Clark, and R. L. Mercer, Phys. Rev. C **37**, 1307 (1988).
- [54] G. W. Hoffmann, L. Ray, M. L. Barlett, R. Ferguson, J. McGill, E. C. Milner, K. K. Seth, D. Barlow, M. Bosko, S. Iverson, M. Kaletka, A. Saha, and D. Smith, Phys. Rev. Lett. **47**, 1436 (1981).
- [55] G. S. Blanpied, G. W. Hoffmann, M. L. Barlett, J. A. McGill, S. J. Greene, L. Ray, O. B. Van Dyck, J. Amann, and H. A. Thiessen, Phys. Rev. C **23**, 2599 (1981).
- [56] L. Ray, G. W. Hoffmann, M. Barlett, J. McGill, J. Amann, G. Adams, G. Pauletta, M. Gazzaly, and G. S. Blanpied, Phys. Rev. C **23**, 828 (1981).
- [57] E. Bleszynski, M. Bleszynski, S. Hajisaeid, G. J. Igo, F. Irom, J. B. McClelland, G. Pauletta, A. Rahbar, A. T. M. Wang, C. A. Whitten, Jr., G. Adams, M. Barlett, G. W. Hoffmann, J. A. McGill, R. Boudrie, and G. Kyle, Phys. Rev. C **25**, 2563 (1982).
- [58] G. W. Hoffmann, L. Ray, M. Barlett, J. McGill, G. S. Adams, G. J. Igo, F. Irom, A. T. M. Wang, C. A. Whitten Jr., R. L. Boudrie, J. F. Amann, C. Glashauser, N. M. Hintz, G. S. Kyle, and G. S. Blanpied, Phys. Rev. C **21**, 1488 (1980).
- [59] I. Slaus, D. J. Margaziotis, R. F. Carlson, W. T. H. Van Oers, and J. R. Richardson, Phys. Rev. C **12**, 1093 (1975).
- [60] J. J. Menet, E. E. Gross, J. J. Malanify, and A. Zucker, Phys. Rev. C **4**, 1114 (1971).
- [61] A. Ingemarsson, J. Nyberg, P. U. Renberg, O. Sundberg, R. F. Carlson, A. Auce, R. Johansson, G. Tibell, B. C. Clark, L. K. Kerr, and S. Hama, Nucl. Phys. A **653**, 341 (1999).
- [62] A. Auce, A. Ingemarsson, R. Johansson, M. Lantz, G. Tibell, R. F. Carlson, M. J. Shachno, A. A. Cowley, G. C. Hillhouse, N. M. Jacobs, J. A. Stander, J. J. van Zyl, S. V. Fortsch, J. J. Lawrie, F. D. Smit, and G. F. Steyn, Phys. Rev. C **71**, 064606 (2005).
- [63] A. E. Taylor and E. Wood, Nucl. Phys. **25**, 642 (1961).
- [64] P. U. Renberg, D. F. Measday, M. Pepin, P. Schwaller, B. Favier, and C. Richard-Serre, Nucl. Phys. A **183**, 81 (1972).
- [65] J. F. Dicello and G. Igo, Phys. Rev. C **2**, 488 (1970).
- [66] R. F. Carlson, A. J. Cox, J. R. Nimmo, N. E. Davison, S. A. Elbakr, J. L. Horton, A. Houdayer, A. M. Sourkes, W. T. H. Van Oers, and D. J. Margaziotis, Phys. Rev. C **12**, 1167 (1975).
- [67] J. F. Turner, B. W. Ridley, P. E. Cavanagh, G. A. Gard, and A. G. Hardacre, Nucl. Phys. **58**, 509 (1964).
- [68] B. D. Anderson, P. R. Bevington, F. H. Cverna, M. W. McNaughton, H. B. Willard, R. J. Barrett, N. S. P. King, and D. J. Ernst, Phys. Rev. C **19**, 905 (1979).
- [69] K. Minomo, K. Ogata, M. Kohno, Y. R. Shimizu, and M. Yahiro, J. Phys. G **37**, 085011 (2010).
- [70] P. D. Greaves, V. Hnizdo, J. Lowe, and O. Karban, Nucl. Phys. A **179**, 1 (1972).
- [71] S. Kato, K. Okada, M. Kondo, K. Hosono, T. Saito, N. Mat-



- suoka, K. Hatanaka, T. Noro, S. Nagamachi, H. Shimizu, K. Ogino, Y. Kadota, S. Matsuki, and M. Wakai, Phys. Rev. C **31**, 1616 (1985).
- [72] G. S. Mani, D. T. Jones, and D. Jacques, Nucl. Phys. A **165**, 384 (1971).
- [73] H. Sakaguchi, M. Nakamura, K. Hatanaka, A. Goto, T. Noro, F. Ohtani, H. Sakamoto, H. Ogawa, and S. Kobayashi, Phys. Rev. C **26**, 944 (1982).
- [74] S. Karataglidis, in private communication.
- [75] N. Matsuoka, M. Kondo, A. Shimizu, T. Saito, and S. Nagamachi, Nucl. Phys. A **345**, 1 (1980).
- [76] A. Auce, R. F. Carlson, A. J. Cox, A. Ingemarsson, R. Johansson, P. U. Renberg, O. Sundberg, and G. Tibell, Phys. Rev. C **53**, 2919 (1996).
- [77] G. P. Millburn, W. Birnbaum, W. E. Crandall, and L. Schecter, Phys. Rev. **95**, 1268 (1954).
- [78] H. An and C. Cai, Phys. Rev. C **73**, 054605 (2006).

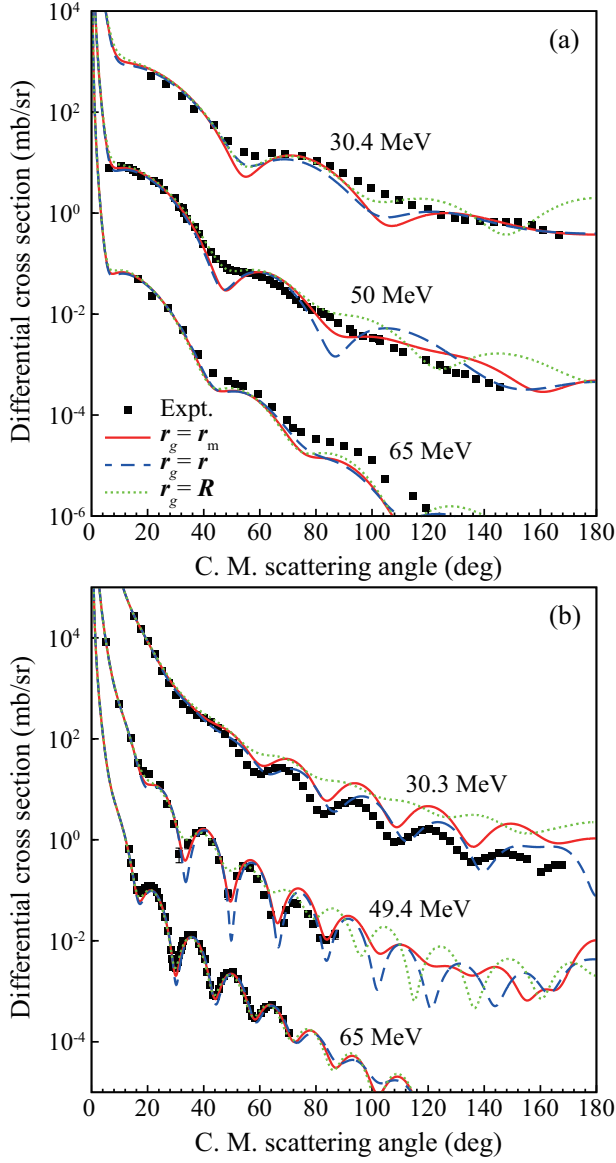


FIG. 8: (Color online) Differential cross sections for a)  $p-^{12}\text{C}$  and b)  $p-^{208}\text{Pb}$  scattering calculated with the different choice of  $r_g$ . The horizontal axis is the scattering angle in the center-of-mass frame. The solid, dashed, and dotted lines correspond to i)  $r_g = r_m$ , ii)  $r_g = r$ , and iii)  $r_g = R$ , respectively. From the top, the incident energies correspond to 30.4, 50, 65 MeV in panel (a), and 30.3, 49.4, 65 MeV in panel (b). The results at higher energies are scaled for visibility. The experimental data are taken from Refs. [42, 49, 70–73].

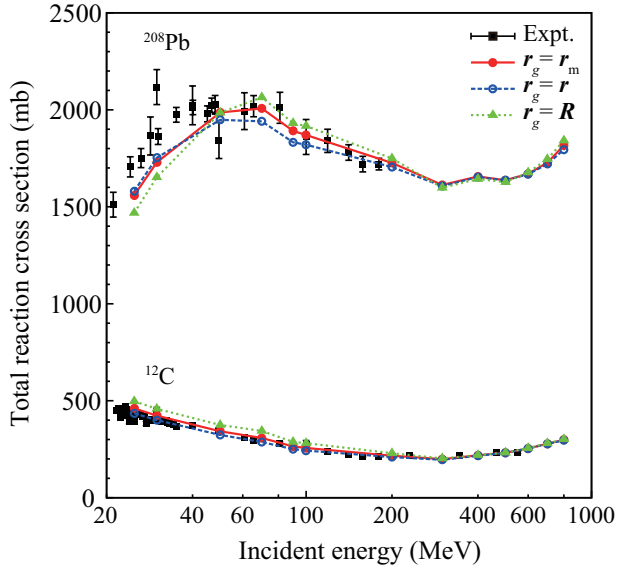


FIG. 9: (Color online) The energy dependence of the total reaction cross sections of  $p$ - $^{12}\text{C}$  and  $p$ - $^{208}\text{Pb}$  scattering. The open circles, the closed circles, and the triangles correspond to choices i), ii), and iii) for  $r_g$ , respectively. The experimental data are same as in Figs. 5 and 7.

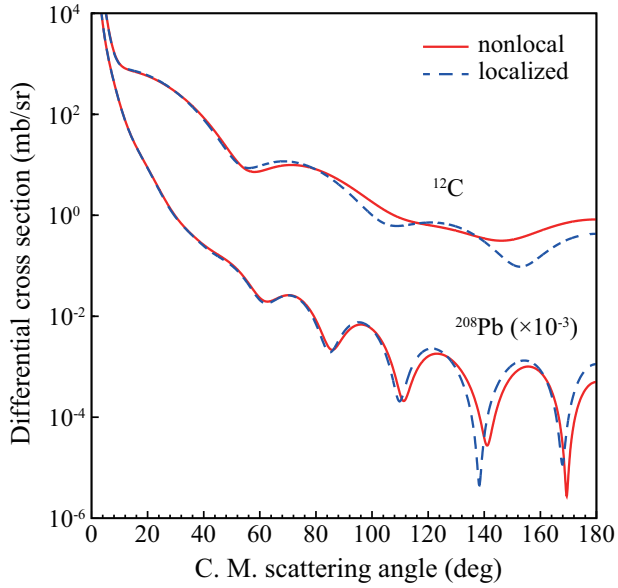


FIG. 10: (Color online) Differential cross sections for  $p$ - $^{12}\text{C}$  and  $p$ - $^{208}\text{Pb}$  at 30 MeV as a function of the center-of-mass scattering angle. The solid (dashed) line is the result with the nonlocal (localized) potential. The results for  $^{208}\text{Pb}$  target are scaled by  $10^{-3}$  for visibility.

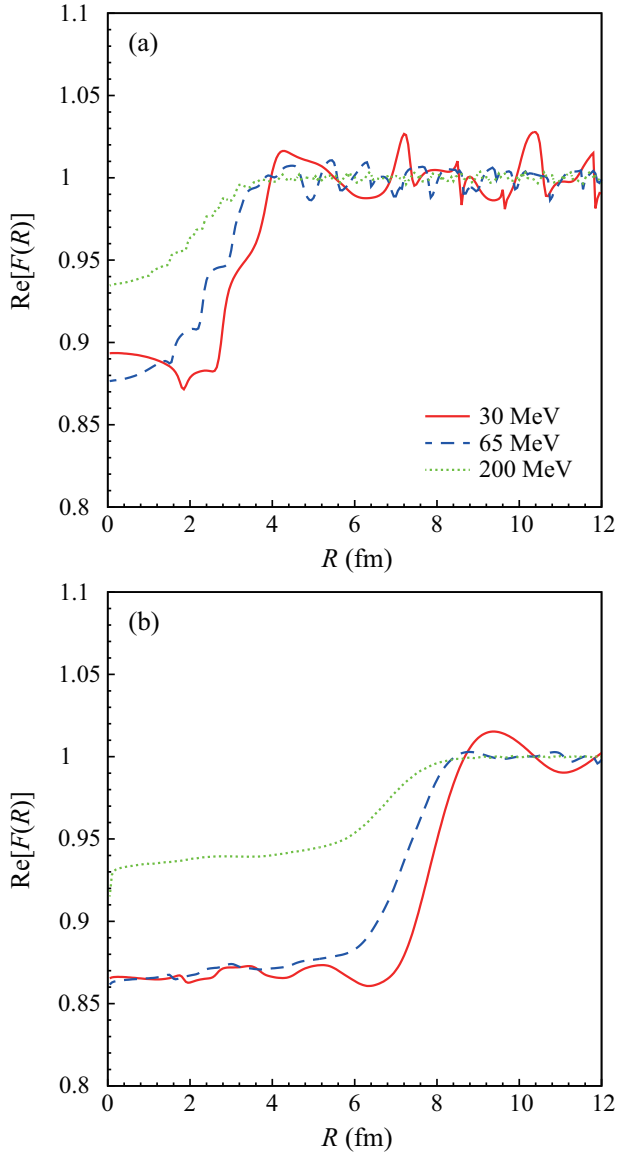


FIG. 11: (Color online) Real part of the averaged Perey factor  $F(R)$  for (a)  $p$ - $^{12}\text{C}$  and (b)  $p$ - $^{208}\text{Pb}$  scattering. The solid, dashed, and dotted lines show the results at 30, 65, and 200 MeV, respectively.

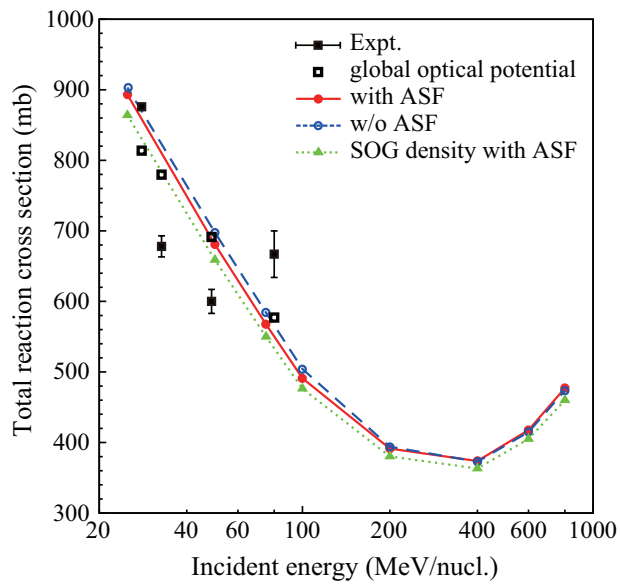


FIG. 12: (Color online) Same as Fig. 5 but for  $d$ - $^{12}\text{C}$ . The experimental data are taken from Refs. [75–77]. The results with the global optical potential for deuteron elastic scattering [78] are shown by the open squares.